Electronic Supplementary Material (ESI) for RSC Advances.

Electronic Supporting Information

Effect of Al content on number and location of hydroxyl acid species in zeolites: A DRIFTS quantitative protocol without the need of molar extinction coefficients

Pierre Bräuer,[a] Pey Ling Ng,[a] Olivia Situmorang,[a] Iain Hitchcock,[b] C. D'Agostino[a,*]

[a] Department of Chemical Engineering and Biotechnology, University of Cambridge, Pembroke Street, Cambridge, CB2 3RA, UK

[b] Johnson Matthey Technology Centre, Blount's Court, Sonning Common, Reading, RG4 9NH, UK

*Corresponding Author:

Dr Carmine D'Agostino

Department of Chemical Engineering & Biotechnology

University of Cambridge

Pembroke Street

Cambridge

CB2 3RA, UK

Email: cd419@cam.ac.uk

Tel: +44(0)1223-761629

S.1. Correlation of zeolite characterisation results

To assess if the BET surface area or crystal size of H-ZSM-5 were Al dependent both characterisation parameters were plotted over the total Al concentration shown in Figure S1. The BET surface area, Figure S1 (left), of the investigated H-ZSM-5 zeolites does not seem to follow a trend associated with the total Al content. Increasing[1] and decreasing[2] trends have been reported. However, in this study the Al concentration is suggested to not have a significant influence on the BET surface area. The H-ZSM-5 crystal size obtained by SEM characterisation experiments, Figure S1 (right), does not seem to vary with the total Al content either.

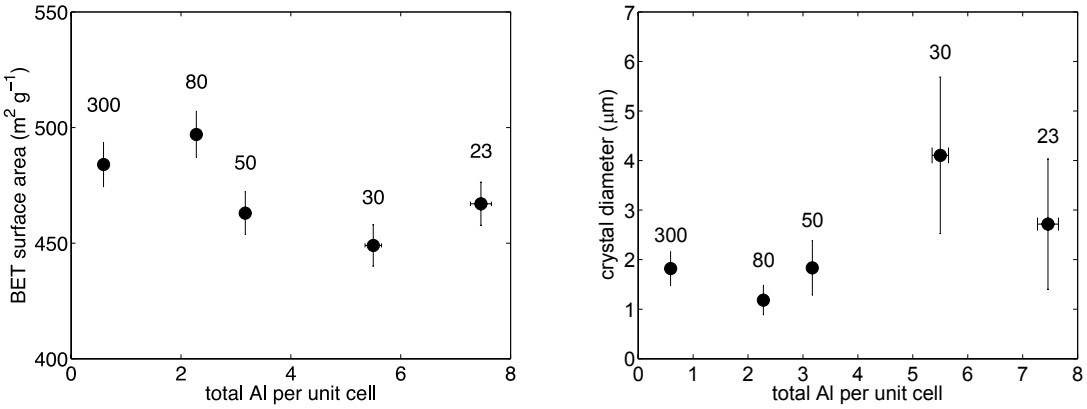

Figure S1. Zeolite characterisation results for **(left)** BET surface area from argon sorption isotherms and **(right)** crystal diameters obtain from SEM characterisation over total Al concentration per unit cell for H-ZSM-5 with different SAR (300, 80, 50, 30 and 23 from left to right). Error bars for BET values were estimated with 2%. Crystal size error bars were calculated based on the standard deviation of a crystal count of 30.

S.2. SEM characterisation

SEM experiments were carried out to investigate typical structural characteristics such as the morphology and crystal size of the H-ZSM-5 samples with varying SAR. The SEM images are shown in Figure S3. Morphological differences can be observed. H-ZSM-5 (23) and H-ZSM-5 (80) consist of clusters formed of cubic structures. However, H-ZSM-5 (80) appears to be more agglomerated than H-ZSM-5 (23). H-ZSM-5 (30) and H-ZSM-5 (50) are agglomerates formed of very fine particles. In contrast to the other four H-ZSM-5 samples H-ZSM-5 (300) has approximately spherical structures that do not seem to be agglomerated. Some additional structures can be identified at higher magnifications.

Values for the average diameter of H-ZSM-5 crystals were obtained from the agglomerated structures observed in Figure S3 rather than on individual crystals as a significantly better correlation was obtained for the former with the BET surface areas as shown in Figure S2. To confirm that the BET surface area and SEM crystal size results are reasonable those two were correlated. Independently of the total Al content the BET surface area should decrease for increasing crystal diameters,[1,3,4] which is the case as shown in Figure S2.

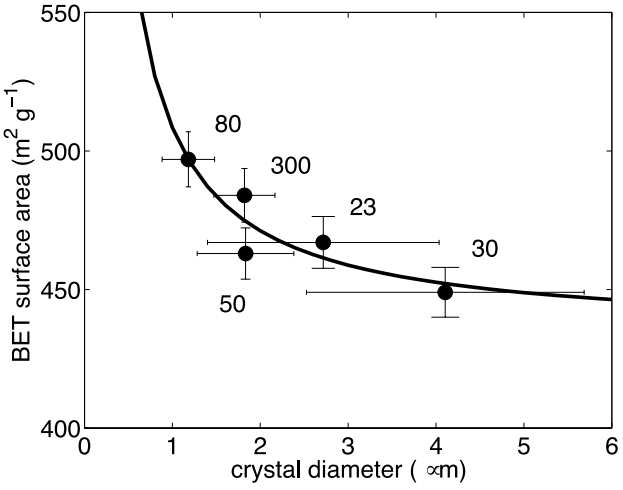

Figure S2. BET surface area from argon sorption isotherms over crystal diameters for H-ZSM-5 zeolites with varying SAR. Solid line serves as guide to the eye and is fit of the data to the equation $y = a\,x^{-1} + b$, where a and b are fitting coefficients, x the crystal diameter and y the BET surface area.

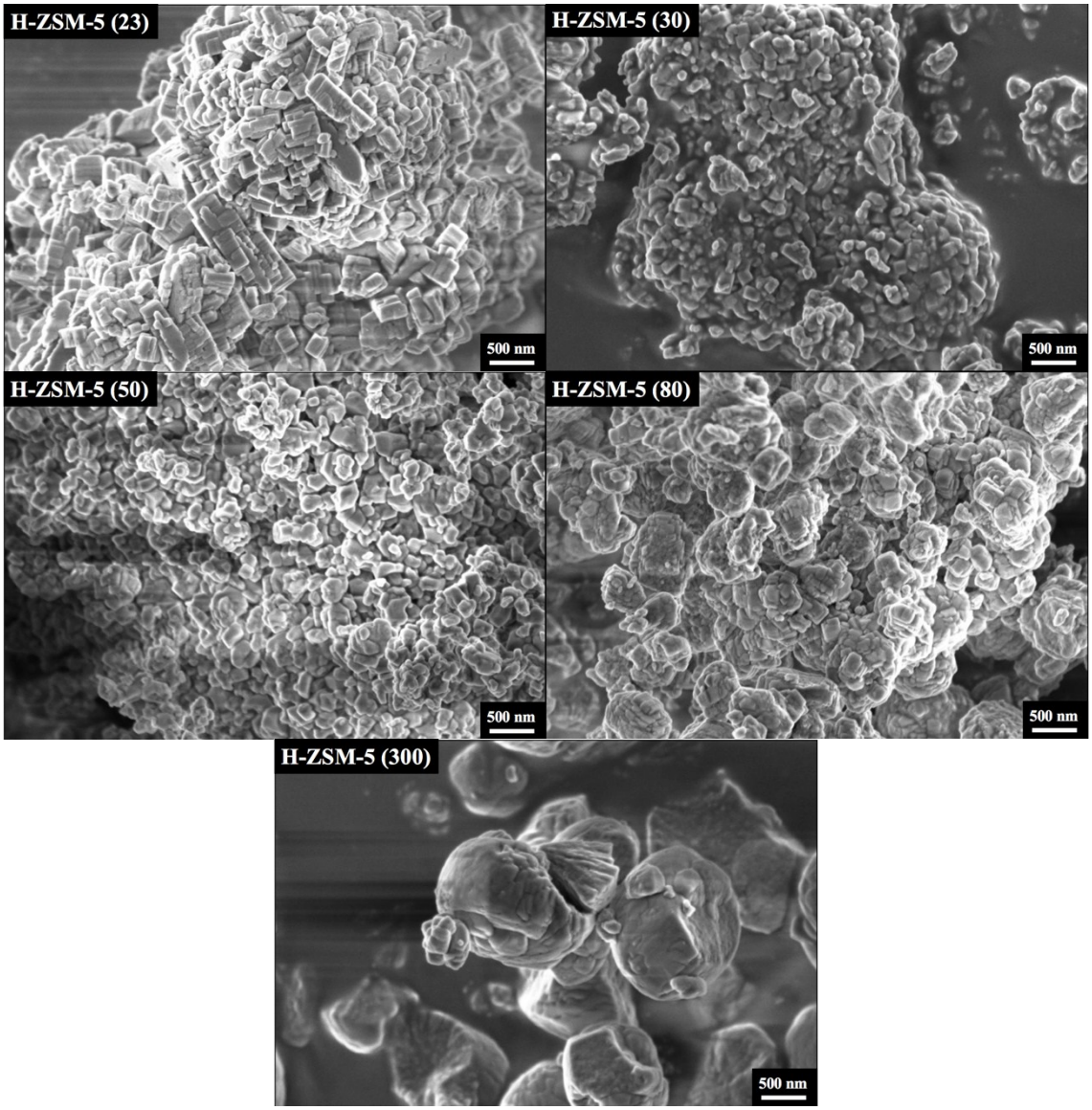

Figure S3. SEM images of H-ZSM-5 crystals with varying SAR.

S.3. Elemental analysis

H-ZSM-5 zeolite samples were exchanged with sodium and characterised by elemental analysis (ICP-MS) together with the proton form. Complete exchange of the sodium cations (Na^+) with the Brønsted protons (H^+) was verified by IR experiments confirming the absence of the Brønsted peak at ~3610 cm^{-1}. From this procedure, the different Al species in the H-ZSM-5 zeolites were calculated.[5] In more detail, during the Na^+ exchange of the H^+ form, any cationic species might be expected to exchange with Na^+. Thus, if there are cationic EF-Al species, Figure S4 (b), sitting where there would otherwise be H^+, Figure S4 (a), these species may also exchange with a Na^+ ion, Figure S4 (c).

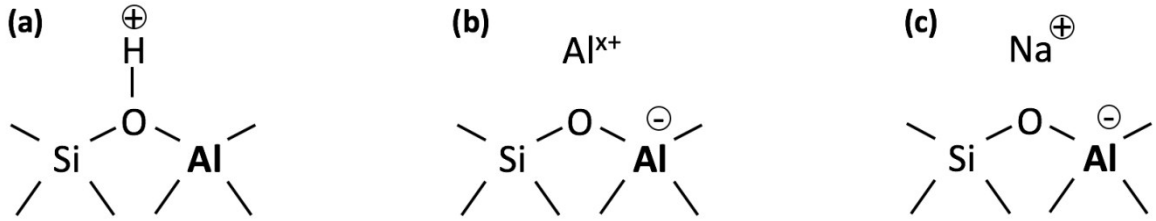

Figure S4. (a) Framework Al atoms compensated in their negative charge by hydroxyl protons, framework Al atoms in the vicinity of **(b)** cationic extra-framework Al atoms and **(c)** extra-framework sodium cations. Adopted from Jiao et al.[6]

There could also be neutral EF-Al species present, such as an amorphous alumina (Al_2O_3) phase. These are insoluble and will not exchange with Na^+. They will instead remain in the sample, but associated Al atoms will not exchange a Na atom because the Al atoms are not associated with an exchangeable cation. In general, the amount of Al in the Na^+ form will be less than or equal to the amount of Al in the H^+ form.

The difference of Al concentration in the proton form, $[Al]_{H\text{-}form}$, and sodium form, $[Al]_{Na\text{-}form}$, respectively, is equal to the amount of Al that was removed during the exchange, presumably in a cationic form:

$$[cationic\ EF-Al] = [Al]_{H-form} - [Al]_{Na-form} \quad (1)$$

The difference between the Al and Na content in the sodium form, $[Al]_{Na\text{-}form}$ and $[Na]_{Na\text{-}form}$, respectively, gives the amount of Al that was not exchanged by Na^+, hence, neutral or Al_2O_3-like species:

$$[neutral\ EF-Al] = [Al]_{Na-form} - [Na]_{Na-form} \quad (2)$$

Finally, the concentration of Brønsted Al can be calculated using the following equation:[5]

$$[H^+]_{H-form} = [total\ Al]_{H-form} - [neutral\ EF-Al] - 2[cationic\ EF-Al] \quad (3)$$

In Equation (3) $[H^+]_{H\text{-}form}$ is the Brønsted Al concentration and $[total\ Al]_{H\text{-}form}$ the total Al concentration in the proton form, respectively. The amount of cationic EF-Al must be subtracted twice because it constitutes an Al atom that is not connected to Brønsted acidity and additionally it poisons a F-Al atom that would normally be associated with a proton. The results of the procedure outlined above are summarised in Table S1.

For comparison, the total Al concentration calculated from the SAR supplied by Alfa Aesar is reported in Table S1 as well. Within the experimental uncertainty, the results for the total Al concentration are in excellent agreement for H-ZSM-5 with SAR values of 23, 80 and 300 and only show a small deviation, that is lower concentration, for H-ZSM-5 with SAR values of 30 and 50.

Table S1. Concentration of total Al calculated from SAR supplied by Alfa Aesar for the NH_4^+ form of ZSM-5 and concentration of total Al, Brønsted Al, EF-Al, cationic EF-Al and neutral EF-Al per unit cell (u.c.) for H-ZSM-5 obtained by elemental analysis of the proton form and sodium form of ZSM-5 with SAR values of 23, 30, 50, 80 and 300, respectively.

SAR[a]	**Al_{total}**[b]	**Al_{total}**[c]	**$Al_{Brønsted\text{-}Al}$**[c]	**$Al_{EF\text{-}Al}$**[c]	**$Al_{EF\text{-}Al,cationic}$**[a]	**$Al_{EF\text{-}Al,neutral}$**[a]
23	7.7	7.5 ± 0.2	6.2 ± 0.6	1.1 ± 0.3	0.2 ± 0.3	0.9 ± 0.1
30	6.0	5.5 ± 0.2	4.3 ± 0.5	1.3 ± 0.2	0	1.3 ± 0.1
50	3.7	3.2 ± 0.1	2.4 ± 0.3	0.7 ± 0.1	0	0.7 ± 0
80	2.3	2.3 ± 0.1	2.0 ± 0.2	0.3 ± 0.1	0	0.2 ± 0
300	0.6	0.6 ± 0	0.5 ± 0.1	0.1 ± 0	0	0.1 ± 0

[a] supplied by Alfa Aesar for the NH_4^+ form of ZSM-5
[b] calculated from SAR supplied by Alfa Aesar
[c] measured by ICP-MS in Al atoms per unit cell (u.c.)

S.4. Quantitative analysis of DRIFTS spectra

The purpose of this section is to determine what conversion function for DRIFTS spectra, absorbance or Kubelka-Munk[7] (KM) function, respectively, gives a linear correlation between DRIFTS signal and the concentration of the surface hydroxyl groups such as Brønsted or terminal silanol acid sites.

Diffuse-reflectance IR spectroscopy has several advantages over the very commonly used transmission IR spectroscopy such as simple sample preparation and better applicability for *in-situ* characterisation at high temperatures and pressures. The biggest disadvantage of diffuse-reflectance IR spectroscopy is that experiments are frequently limited to semi-quantitative analyses. However, quantitative IR data analysis is required when the surface concentration and its trend are to be probed. In the best-case scenario, the IR intensity of DRIFTS data is proportional to the concentration of the adsorbed probe molecule. To obtain IR band intensities that are linear to the surface concentration of adsorbed species the KM function is frequently applied to the diffuse-reflectance IR data yielding a linear[8] calibration curve:

$$KM = f(R_\infty) = \frac{(1 - R_\infty)^2}{2R_\infty} = \frac{k}{s} \tag{S4}$$

The absolute reflectance (R_∞) of the scattered radiation is related to the sample absorption coefficient (k) and the scattering coefficient (s) by the KM function. R_∞ is defined by the scattered intensity divided by the incident radiation and is a function of the wavenumber. The incident radiation is normally not known. Thus, a typical DRIFTS experiment consists of first probing the reflectance I_∞(reference) over highly scattering and poorly absorbing particles as a reference (e.g., KBr powder). After, the reflectance of the sample of interest itself I_∞(sample) is determined. The following ratio is then taken as an estimate for the absolute reflectance (R_∞):

$$R_\infty \approx \frac{I_\infty(sample)}{I_\infty(reference)} \tag{S5}$$

However, transforming the acquired DRIFTS data using the KM function curved[9–11] or broken-line shape[12] calibration curves have been reported as well. For strongly absorbing materials it has been suggested[10] that the best approximation for the calibration curve can be obtained by calculating the absorbance defined as

$$Absorbance = log\left(\frac{1}{R_\infty}\right) \quad \text{(S6)}$$

in which R_∞ is the absolute reflectance as defined earlier used in the KM function in (S4). This approach is in analogy to the absorbance measured in transmission mode given by log (1/T), where T stands for transmission. Both functions, absorbance and KM, are frequently used to linearise the diffuse-reflectance IR intensities. The reasoning for selecting either one is normally not discussed. This is often the case as it is difficult to measure the amount of probe molecule uptake and the diffuse-reflectance IR intensities simultaneously.

To confirm that the DRIFTS setup gives a linear correlation between IR intensities and the concentration of surface hydroxyls, the absorbance, equation (S6), and KM function, equation (S4), were used to transform the acquired raw diffuse-reflectance IR data to absorbance and KM spectra, respectively. The Brønsted peak in the O-H stretching region was then integrated for both conversion functions and all five SARs of H-ZSM-5, respectively. All Brønsted peak areas were normalised by the peak areas of the framework vibrations between 1750 and 2100 cm^{-1}. The concentration of Brønsted Al atoms was independently determined by elemental analysis of the H-form and Na-form of the same ZSM-5 zeolites. To test the linear correlation between DRIFTS signal and surface hydroxyl concentration the integrated and normalised Brønsted absorbance and KM areas were then plotted over the Brønsted Al concentration obtained by elemental analysis, depicted in Figure S5.

The absorbance function illustrated in Figure S5 (left) shows a good agreement between the integrated Brønsted peak area and the Brønsted Al concentration determined by elemental analysis characterisation. Within the experimental error the integrated Brønsted peak area increases linearly with the Brønsted Al concentration. This suggests that the absorbance function is suitable to quantitatively probe the number Brønsted hydroxyl groups in the O-H stretching region and thus likely also the number of terminal silanol sites. However, an independent measurement of the latter was not available. The fitting gives a molar extinction coefficient (ε) of $(2.12 \pm 0.10) \times 10^{-4}$ cm μmol^{-1}, which can be used to calculate the Brønsted Al concentration and its change as a first approximation.

The results for the integrated Brønsted peak area using the KM function plotted over the Brønsted Al concentration determined from elemental analysis is depicted in Figure S5 (right). The correlation is significantly worse and particularly the data point for H-ZSM-5 (23) is too high compared to the other four data points. Hence, the KM function does not seem to be a good choice to quantitatively probe the number of Brønsted hydroxyl groups. In

conclusion, the results obtained for the absorbance and KM calibration curves suggest that absorbance function is the better choice to interpret the diffuse-reflectance IR data quantitatively.

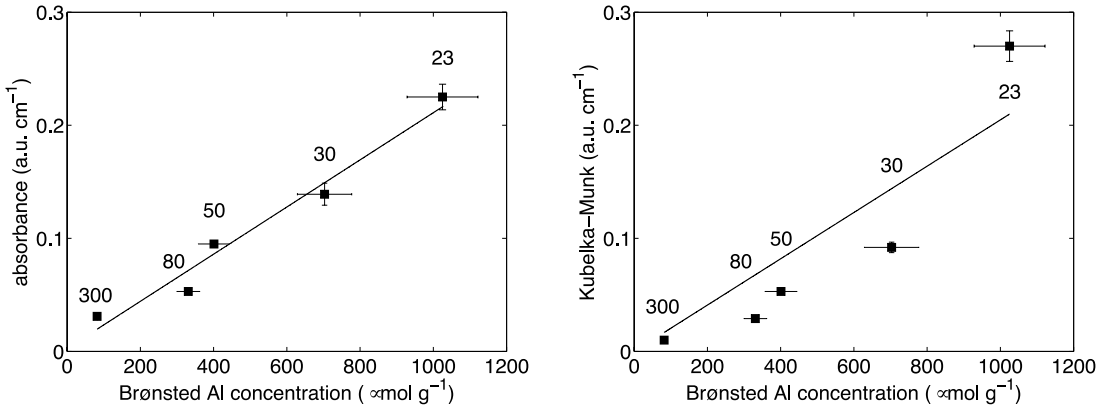

Figure S5. Framework vibration normalised areas of activated Brønsted IR peak (~3610 cm^{-1}) for **(left)** absorbance function and **(right)** KM function over Brønsted Al concentration obtained by elemental analysis of H-form and Na-form of ZSM-5 with different SAR (300, 80, 50, 30 and 23 from left to right) at 300 K. Straight line represents fit to linear equation.

Some IR studies have reported that diffuse-reflectance experiments are strongly affected by particle size and packing density of the sample bed leading to significant errors due to experimental results not being reproducible.[8,13] However, the results presented in Figure S5 (left) show that the errors for the Brønsted IR peaks exhibit a maximum value of 5% determined by repeating the experiments three times. Hence, the normalisation by the area of the framework vibrations seems to consider the different sample weights. Furthermore, the particle size of the H-ZSM-5 samples ranges from 1.18 to 4.10 μm suggesting that the particle size does not significantly affect the results.

In summary, it has been shown that the absorbance function performs better in giving a linear DRIFTS signal intensity for the Brønsted hydroxyls in the O-H stretching region.

S.5. Statistical data

The Table S2 reports the data plotted in Figure 4 in the paper, that is, the variation of the normalised Brønsted peak area before probe molecule adsorption with total Al concentration.

Table S2. Mean value ($\bar{x}$) and standard deviation (σ) of total Al concentration per unit cell obtained from elemental analysis and normalised area of activated Brønsted IR peak (~3610 cm^{-1}), that is, before probe molecule adsorption, for SAR of 23, 30, 50, 80 and 300.

SAR[a]	total Al[b]		IR area[c]	
	$\bar{x}$	σ	$\bar{x}$	σ
23	7.5	0.2	0.225	0.011
30	5.5	0.2	0.139	0.010
50	3.2	0.1	0.095	0.001
80	2.3	0.1	0.053	0.003
300	0.6	0	0.031	0.003

[a] supplied by Alfa Aesar for the NH_4^+ form of ZSM-5
[b] total Al concentration measured by ICP-MS in Al atoms per unit cell (u.c.)
[c] normalised activated Brønsted IR peak (a.u. cm^{-1})

The Table S3 reports the data plotted in Figure 7 in the paper, that is, the variation of the normalised Brønsted peak area before collidine adsorption, after collidine adsorption and the difference between the two (area reduction Δ) with F-Al concentration.

Table S3. Mean value ($\bar{x}$) and standard deviation (σ) of framework Al concentration per unit cell obtained from elemental analysis and normalised area of Brønsted peak prior to collidine adsorption, after collidine adsorption and the difference between the two, that is, the area reduction (Δ), for SAR of 23, 30, 50, 80 and 300.

SAR[a]	F-Al[b]		IR $area_{prior}$[c]		IR $area_{after}$[d]		IR $area_{\Delta}$[e]	
	$\bar{x}$	σ	$\bar{x}$	σ	$\bar{x}$	σ	$\bar{x}$	σ
23	6.4	0.4	0.225	0.011	0.245	0.012	0.059	0.003
30	4.3	0.3	0.139	0.010	0.144	0.007	0.057	0.003
50	2.4	0.2	0.095	0.001	0.061	0.003	0.038	0.002
80	2.0	0.1	0.053	0.003	0.039	0.002	0.019	0.001
300	0.5	0	0.031	0.003	0.015	0.001	0.011	0.001

[a] supplied by Alfa Aesar for the NH_4^+ form of ZSM-5
[b] framework Al (F-Al) concentration measured by ICP-MS in Al atoms per unit cell (u.c.)
[c] normalised area of Brønsted IR peak (a.u. cm^{-1}) prior to collidine adsorption
[d] normalised area of Brønsted IR peak (a.u. cm^{-1}) after to collidine adsorption
[e] area reduction of Brønsted IR peak (a.u. cm^{-1})

The Table S4 reports the data plotted in Figure 8 in the paper, that is, the variation of the percentage of Brønsted peak area accessible to collidine with F-Al concentration.

Table S4. Mean value ($\bar{x}$) and standard deviation (σ) of framework Al concentration per unit cell obtained from elemental analysis and percentage of Brønsted peak area accessible to collidine for SAR of 23, 30, 50, 80 and 300.

SAR[a]	**F-Al**[b]		**accessible to collidine**[c]	
	$\bar{x}$	σ	$\bar{x}$	σ
23	6.4	0.4	19.1	0.4
30	4.3	0.3	27.6	0.6
50	2.4	0.2	34.3	1.7
80	2.0	0.1	30.4	1.3
300	0.5	0	34.6	6.8

[a] supplied by Alfa Aesar for the NH_4^+ form of ZSM-5
[b] framework Al (F-Al) concentration measured by ICP-MS in Al atoms per unit cell (u.c.)
[c] percentage of Brønsted peak area accessible to collidine

S.6. Spectra in OH region after probe molecule adsorption

The IR spectra of H-ZSM-5 after probe molecule adsorption, that is, after pyridine or collidine adsorption, are depicted in the OH region from 3000 to 4000 cm^{-1} in Figure S6.

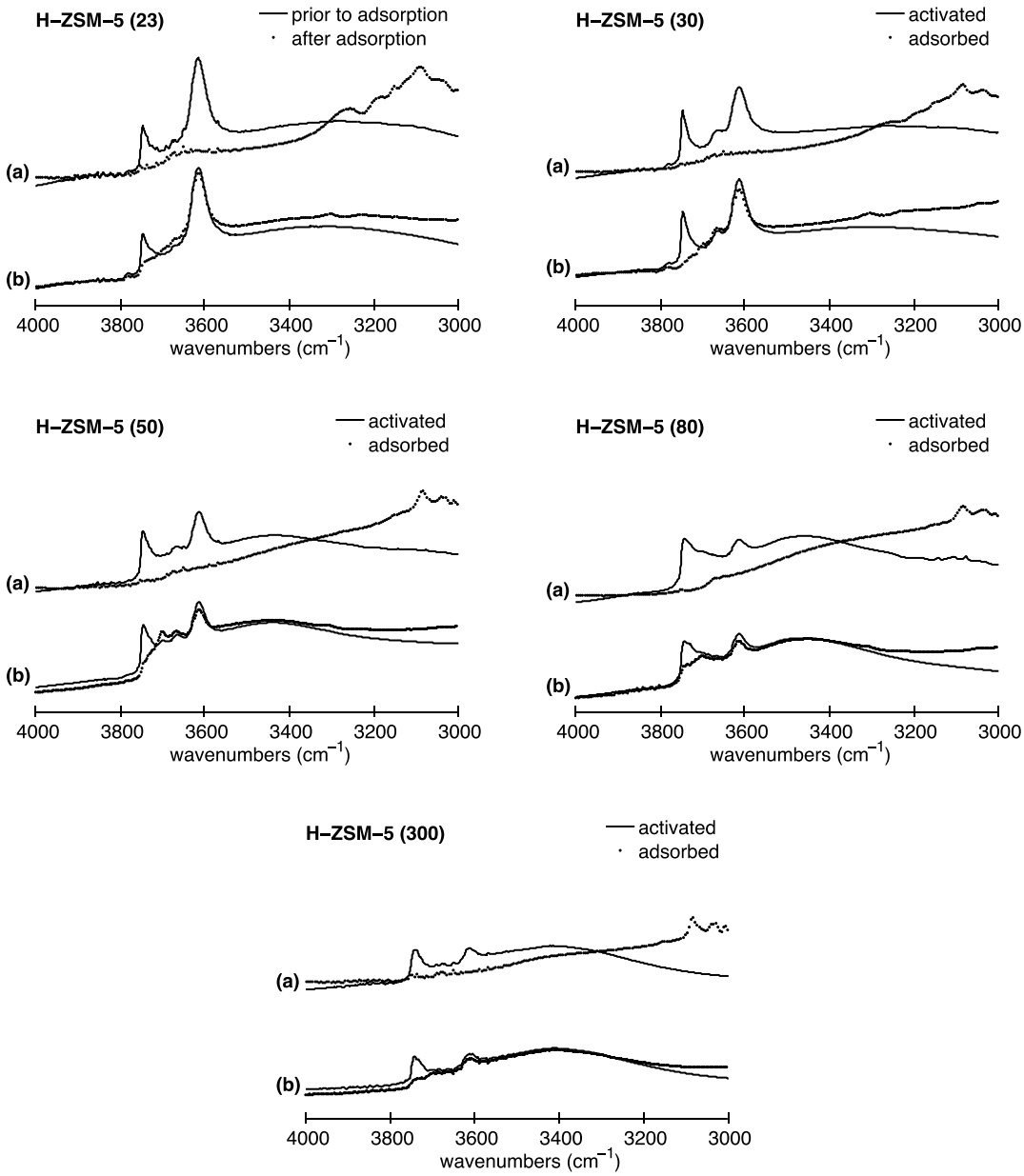

Figure S6. Normalised IR spectra of H-ZSM-5 with SAR values of 23, 30, 50, 80 and 300, respectively, for **(a)** pyridine and **(b)** collidine adsorption in the O-H stretching region (3000 to 4000 cm^{-1}): **(solid line)** spectrum prior to probe molecule adsorption, **(filled circles)** spectrum after probe molecule adsorption. The *y*-axis (absorbance a.u.) in each plot has the same scale so spectra can directly be compared.

S.7. Adsorbed probe molecule IR spectra

The IR spectra of the adsorbed probe molecules pyridine and collidine are illustrated in the following plots Figure S7 and Figure S8, respectively.

Figure S7 illustrates the framework vibration normalised IR spectra of H-ZSM-5 upon pyridine adsorption between 1400 and 1700 cm^{-1}. The peak at ~1445 cm^{-1}, commonly assigned to pyridine interacting with Lewis acid sites,[14,15] can be observed in all five H-ZSM-5 zeolites. Another peak or shoulder, depending on the SAR, can be observed at ~1440 cm^{-1} suggesting a slightly different type of Lewis acid site. Interestingly, a third peak can further be identified for all five investigated SARs at ~1454 cm^{-1}. Hence, the pyridine adsorption results suggest the presence of two main types of Lewis acid sites. The first two peaks at ~1440 and 1445 cm^{-1}, respectively, have been assigned to weaker Lewis acid sites originating from EF-Al.[16] The presence of EF-Al is frequently thought to give rise to Lewis acidity. However, not every EF-Al species acts as a Lewis acid site as neutral EF-Al can constitute amorphous alumina (Al_2O_3) phase.[6] The third peak (~1454 cm^{-1}) has been assigned to a stronger type of Lewis acid site believed to originate from electronic defaults in the F-Al.[16,17] The peak at ~1545 cm^{-1}, commonly assigned to pyridine interacting with Brønsted acid sites,[18] is most pronounced for H-ZSM-5 (23) and decreases with increasing SAR, that is, decreasing total Al content. The third indicated peak at ~1490 cm^{-1} represents both pyridine molecules interacting with Lewis and Brønsted acid sites.[19]

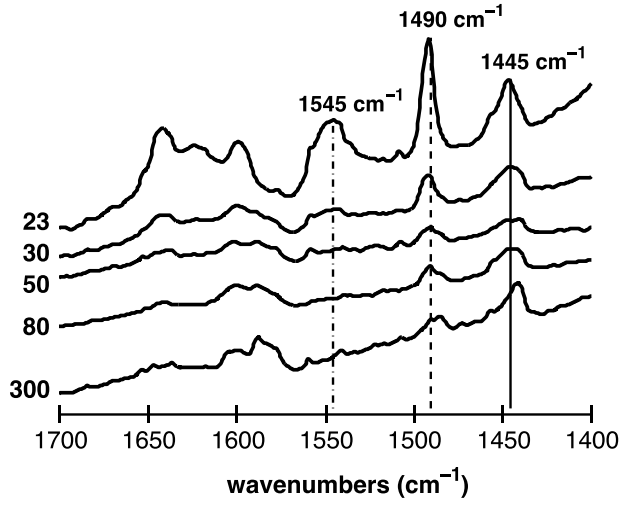

Figure S7. Framework vibration normalised IR spectra of pyridine adsorbed in H-ZSM-5 with a SAR of 23, 30, 50, 80 and 300 (indicated in the plot) between 1400 and 1700 cm^{-1} at 300 K. The *y*-axis (absorbance) has arbitrary units. Lines indicate the peaks assigned to pyridine interacting with Lewis acid sites (solid line at ~1445 cm^{-1}), Lewis and Brønsted acid sites (dashed line at ~1490 cm^{-1}) and Brønsted acid sites (dash-dot lines at ~1545 cm^{-1}).

Figure S8 illustrates the framework vibration normalised IR spectra of H-ZSM-5 upon collidine adsorption between 1575 to 1675 cm^{-1}. The peak ~1633 cm^{-1} has been assigned and used to probe collidine interacting with Lewis acid sites.[20,21] Collidine molecules interacting with Brønsted acid sites give rise to a peak at ~1636 cm^{-1} and additionally at ~1646 cm^{-1} both indicating the presence of collidinium ions, hence, collidine molecules protonated by Brønsted acid sites.[20–22] Hence, the identification of the external Lewis acid sites using collidine as a base probe molecule can be problematic as the peaks are not well separated. Finally, two further peaks can be identified in Figure S8 at ~1575 and ~1617 cm^{-1}, respectively, both indicating the interaction of collidine molecules with terminal silanol sites.

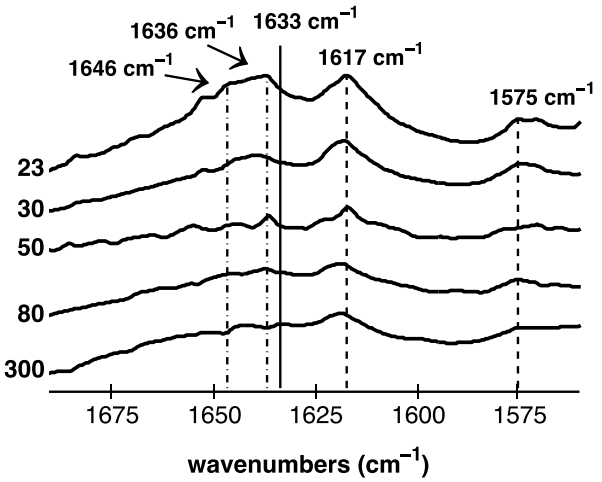

Figure S8. Framework vibration normalised IR spectra of collidine adsorbed in H-ZSM-5 with a SAR of 23, 30, 50, 80 and 300 (indicated in the plot) between 1575 and 1675 cm^{-1} at 300 K. The *y*-axis (absorbance) has arbitrary units. Lines indicate the peaks assigned to collidine interacting with terminal silanol sites (dashed lines at ~1575 and ~1617 cm^{-1}), Lewis acid sites (solid line at ~1633 cm^{-1}) and Brønsted acid sites (dash-dot lines at ~1636 and ~1646 cm^{-1}).

References

1 T. Armaroli, L. J. Simon, M. Digne, T. Montanari, M. Bevilacqua, V. Valtchev, J. Patarin and G. Busca, *Applied Catalysis A: General*, 2006, **306**, 78–84.
2 L. Shirazi, E. Jamshidi and M. R. Ghasemi, *Cryst. Res. Technol.*, 2008, **43**, 1300–1306.
3 R. M. Mohamed, O. A. Fouad, A. A. Ismail and I. A. Ibrahim, *Materials Letters*, 2005, **59**, 3441–3444.
4 O. A. Fouad, R. M. Mohamed, M. S. Hassan and I. A. Ibrahim, *Catalysis Today*, 2006, **116**, 82–87.
5 A. Janda and A. T. Bell, *J. Am. Chem. Soc.*, 2013, **135**, 19193–19207.
6 J. Jiao, J. Kanellopoulos, W. Wang, S. S. Ray, H. Foerster, D. Freude and M. Hunger, *Phys. Chem. Chem. Phys.*, 2005, **7**, 3221–3226.
7 P. Kubelka, *J. Opt. Soc. Am., JOSA*, 1948, **38**, 448–457.
8 D. Chen, S. Sharma, N. Cardona-Martínez, J. A. Dumesic, V. A. Bell, G. D. Hodge and R. J. Madon, *Journal of Catalysis*, 1992, **136**, 392–402.
9 M. P. Fuller and P. R. Griffiths, *Anal. Chem.*, 1978, **50**, 1906–1910.
10 J. M. Olinger and P. R. Griffiths, *Anal. Chem.*, 1988, **60**, 2427–2435.
11 F. Boroumand, J. E. Moser and H. van den Bergh, *Appl. Spectrosc., AS*, 1992, **46**, 1874–1886.
12 M. T. McKenzie and J. L. Koenig, *Applied Spectroscopy*, 1985, **39**, 408–412.
13 T. J. Horr, J. Ralston and R. S. C. Smart, *Colloids and Surfaces*, 1992, **64**, 67–85.
14 E. P. Parry, *Journal of Catalysis*, 1963, **2**, 371–379.
15 A. Auroux, V. Bolis, P. Wierzchowski, P. C. Gravelle and J. C. Vedrine, *J. Chem. Soc., Faraday Trans. 1*, 1979, **75**, 2544–2555.
16 J. P. Marques, I. Gener, P. Ayrault, J. C. Bordado, J. M. Lopes, F. R. Ribeiro and M. Guisnet, *Comptes Rendus Chimie*, 2005, **8**, 399–410.
17 N. Brodu, M.-H. Manero, C. Andriantsiferana, J.-S. Pic and H. Valdés, *Chemical Engineering Journal*, 2013, **231**, 281–286.
18 J. C. Védrine, A. Auroux, V. Bolis, P. Dejaifve, C. Naccache, P. Wierzchowski, E. G. Derouane, J. B. Nagy, J.-P. Gilson, J. H. C. van Hooff, J. P. van den Berg and J. Wolthuizen, *Journal of Catalysis*, 1979, **59**, 248–262.
19 A. Maijanen, E. G. Derouane and J. B. Nagy, *Applied Surface Science*, 1994, **75**, 204–212.
20 F. Thibault-Starzyk, A. Vimont and J.-P. Gilson, *Catalysis Today*, 2001, **70**, 227–241.
21 M. S. Holm, S. Svelle, F. Joensen, P. Beato, C. H. Christensen, S. Bordiga and M. Bjørgen, *Applied Catalysis A: General*, 2009, **356**, 23–30.
22 K. Mlekodaj, K. Tarach, J. Datka, K. Góra-Marek and W. Makowski, *Microporous and Mesoporous Materials*, 2014, **183**, 54–61.